Quaternary Science Reviews 270 (2021) 107188

Contents lists available at ScienceDirect

Quaternary Science Reviews

journal homepage: www.elsevier.com/locate/quascirev

Deglacial trends in Indo-Pacific warm pool hydroclimate in an isotope-enabled Earth system model and implications for isotope-based paleoclimate reconstructions

Xiaojing Du [a, b, *], James M. Russell [a, b], Zhengyu Liu [c], Bette L. Otto-Bliesner [d], Yu Gao [e], Chenyu Zhu [f], Delia W. Oppo [g], Mahyar Mohtadi [h], Yan Yan [i], Valier V. Galy [j], Chengfei He [c]

[a] Department of Earth, Environmental, and Planetary Sciences, Brown University, Providence, RI, USA
[b] Institute at Brown for Environment and Society, Brown University, Providence, RI, USA
[c] Atmospheric Science Program, Department of Geography, The Ohio State University, Columbus, OH, USA
[d] Climate and Global Dynamics Laboratory, National Center for Atmospheric Research, Boulder, CO, USA
[e] Department of Atmospheric and Oceanic Sciences, School of Physics, Peking University, Beijing, China
[f] Key Laboratory of Physical Oceanography, Ocean University of China, Qingdao, China
[g] Geology and Geophysics Department, Woods Hole Oceanographic Institution, Woods Hole, MA, USA
[h] MARUM-Center for Marine Environmental Sciences, University of Bremen, Bremen, Germany
[i] Key Laboratory of Ocean and Marginal Sea Geology, Guangzhou Institute of Geochemistry, Chinese Academy of Sciences, Guangzhou, China
[j] Department of Marine Chemistry and Geochemistry, Woods Hole Oceanographic Institution, Woods Hole, MA, USA

ARTICLE INFO

Article history:
Received 24 May 2021
Received in revised form
21 August 2021
Accepted 5 September 2021
Available online xxx

Handling Editor: I Hendy

Keywords:
Indo-Pacific warm pool
Last deglaciation
Precipitation isotopic composition
Land-sea configuration
NW Australian shelf
Indian ocean dipole pattern

ABSTRACT

The Indo-Pacific Warm Pool (IPWP) is the largest source of atmospheric heating and moisture on Earth, energizing the global moisture and energy budgets and controlling global ocean-atmosphere circulation. However, the mechanisms driving orbital-scale changes in hydroclimate and proxy records of precipitation isotopic composition remain poorly known. Here, we use the isotope-enabled Transient Climate Evolution (iTRACE) experiment to investigate long-term hydroclimate and precipitation isotope changes in the IPWP during the last deglaciation, and their response to different climate forcings (sea level and ice sheet, greenhouse gases, orbital forcing, and meltwater flux). The simulations suggest land-sea configuration as the main factor driving long-term hydroclimate and precipitation isotope changes. The exposure of NW Australian shelf (before 14 ka) excited Bjerknes feedbacks across the equatorial Indian Ocean (IO), leading to a warm/wet western IO and cool/dry eastern IO dipole pattern, with overall drying and more enriched precipitation isotopic compositions over the Maritime Continent. However, the exposed Sunda Shelf and the main body of Sahul Shelf (before 12 ka) experienced locally dry conditions but more depleted precipitation isotopic compositions. Greenhouse gases and orbital forcing contribute to a weaker hydroclimate dipole pattern that opposes the effects of NW Australian shelf exposure. Different regions within the IPWP have different simulated sensitivities to these forcings. The heterogeneous responses of precipitation to different forcings across the Maritime Continent and location-dependent relationships between precipitation and its isotopic composition result from a variety of regional climatological processes and may explain the heterogeneity of isotopic records of hydroclimate around the IPWP.

1. Introduction

The Indo-Pacific Warm Pool (IPWP) is the major source of heat and moisture to the Earth's atmosphere. Intense atmospheric convection over the IPWP energizes the Earth's moisture and energy budgets, drives global ocean-atmosphere circulation, and therefore exerts significant influence on global climate (Chiang, 2009). Despite the global importance of the IPWP, past hydroclimate variations and their associated climate forcings remain unclear. The last deglaciation was an interval of global warming

* Corresponding author. Institute at Brown for Environment and Society, Brown University, Providence, RI, USA.
E-mail address: xiaojing_du@brown.edu (X. Du).

https://doi.org/10.1016/j.quascirev.2021.107188
0277-3791/

from the end of the Last Glacial Maximum (LGM) to the early Holocene, when changes in insolation triggered large shifts in the Earth's climate, ice sheets, atmospheric greenhouse gas concentrations (GHGs), and other associated feedbacks (Clark et al., 2012). Understanding how these climate forcings and feedbacks influence long-term hydroclimate changes in the IPWP during the deglaciation will shed light on regional and global climate dynamics.

Paleoclimate modeling studies suggest that a variety of forcings could have influenced IPWP hydroclimate during the last deglaciation, including changes in global temperature and atmospheric greenhouse gases (GHGs) (Boos, 2012), orbitally-forced insolation (Clement et al., 2004), high-latitude ice sheet forcing (Chiang and Bitz, 2005), and inundation of Sunda and Sahul shelves due to rising sea level (Di Nezio et al., 2016; DiNezio et al., 2011, 2018; DiNezio and Tierney, 2013). Proxy records based upon the oxygen and hydrogen isotopic composition of precipitation ($\delta^{18}O_{precip}$, δD_{precip}) preserved in marine and terrestrial paleoclimate archives (e.g. speleothems and lake sediments) have been used to infer hydroclimate variations and test the IPWP response to these forcings (Fig. 1). However, precipitation changes inferred from these isotope records exhibit considerable heterogeneity (Fig. 2). Isotopic shifts recorded from the northern and southern peripheries of the Australian-Indonesian monsoon domain suggest changes in local insolation driven by orbital precession as the dominant control on precipitation (Ayliffe et al., 2013; Meckler et al., 2012). A multiproxy record off southwestern Sumatra suggests the exposure of the IPWP shelves triggered regional drying, potentially due to changes in the Walker circulation across the Indian Ocean (IO) (Windler et al., 2019, 2020). Speleothem records from southwest Sulawesi (Fig. 2b) and western Flores indicate depleted precipitation isotopes during the early Holocene relative to the LGM, also attributed to flooding of Sunda and Sahul shelves (Griffiths et al., 2009; Krause et al., 2019). In contrast, precipitation reconstructions based on leaf wax δD preserved in marine sediment off NW Sumatra suggest little change in rainfall between the LGM and the Holocene (Fig. 2e) (Niedermeyer et al., 2014), or even increased rainfall during the LGM compared to the late Holocene (Mohtadi et al., 2017). Isotopically depleted precipitation during the LGM recorded from offshore East Java (Fig. 2f) (Ruan et al., 2019) and Lake Towuti in eastern Sulawesi (Fig. 2d) (Konecky et al., 2016) are inferred to indicate monsoon intensification and/or seasonal precipitation changes.

The discrepancy among these water isotope records could reflect variable regional sensitivities to different climate forcings. However, the heterogeneous isotopic responses preserved in isotope records (e.g. speleothem $\delta^{18}O$ and leaf wax δD) stand in contrast to widespread LGM drying over IPWP inferred from a variety of other geological and paleocological proxies (e.g. lake level, charcoal, and pollen), especially over the central Indonesia (DiNezio and Tierney, 2013; DiNezio et al., 2018; Reeves et al., 2013; Russell et al., 2014). Moreover, many of the isotopic records infer changes in precipitation amount in this region based upon the "amount effect" (Dansgaard, 1964; Rozanski et al., 1993), which describes a range of processes that result in depleted $\delta^{18}O_{precip}$ and δD_{precip} values with increased precipitation (Emile-Geay et al., 2017; Konecky et al., 2019). Modern observations do show a negative correlation between precipitation isotopic composition and amount at many locations in the IPWP (e.g. Kurita et al., 2009), but both observations and modeling studies suggest that moisture source also has important influence on $\delta^{18}O_{precip}$ in IPWP. For example, Konecky et al. (2016) reported more depleted δD_{precip} recorded from Lake Towuti sediments during the LGM dry condition and suggested that this resulted from intensified Australian-Indonesian summer monsoon circulation, which brings D-depleted precipitation to this region in the present day. However, the impacts of moisture source and amount effects on $\delta^{18}O_{precip}$ and δD_{precip} records remains difficult to constrain from proxy reconstructions alone.

Here we investigate hydroclimate and water isotope changes in

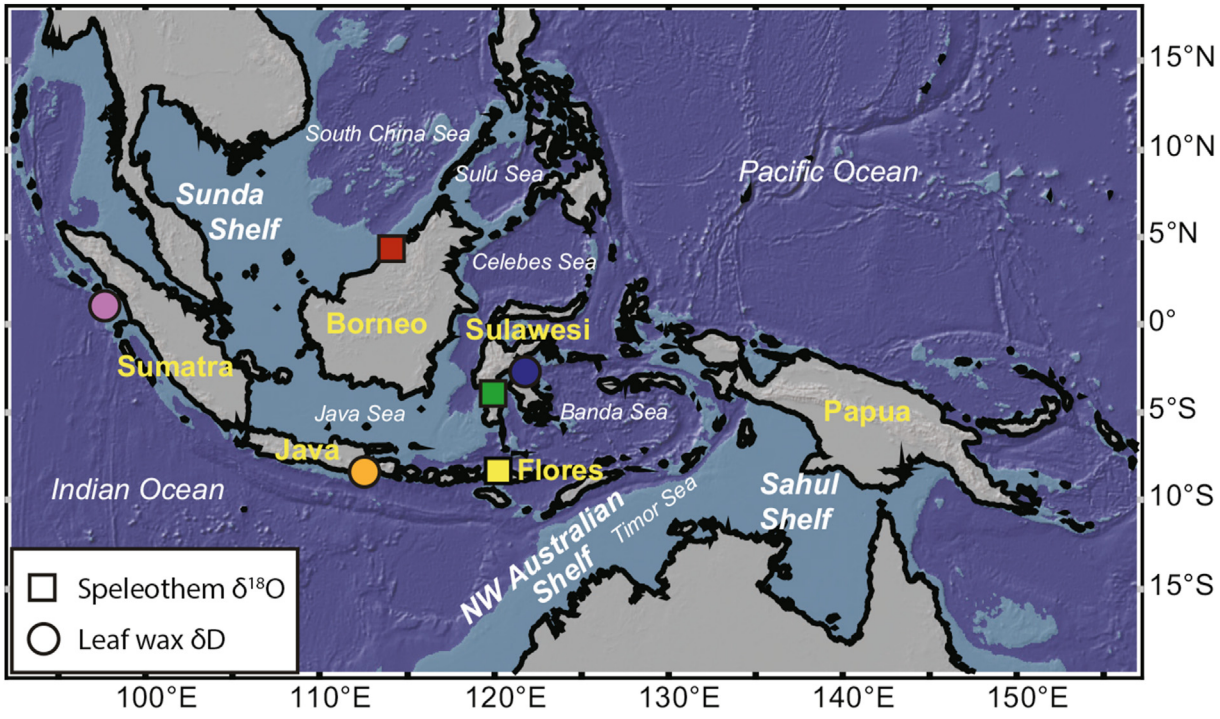

Fig. 1. Map of Maritime Continent showing the location of selected previously published proxy records: speleothem $\delta^{18}O$ from Borneo (Partin et al., 2007), leaf wax δD from northwest Sumatra (Niedermeyer et al., 2014), leaf wax δD from Lake Towuti (Konecky et al., 2016), leaf wax δD from east Java (Ruan et al., 2019), speleothem $\delta^{18}O$ from Sulawesi (Krause et al., 2019), and speleothem $\delta^{18}O$ from Flores (Ayliffe et al., 2013). The location of Sunda, Sahul, and NW Australian shelves are also shown.

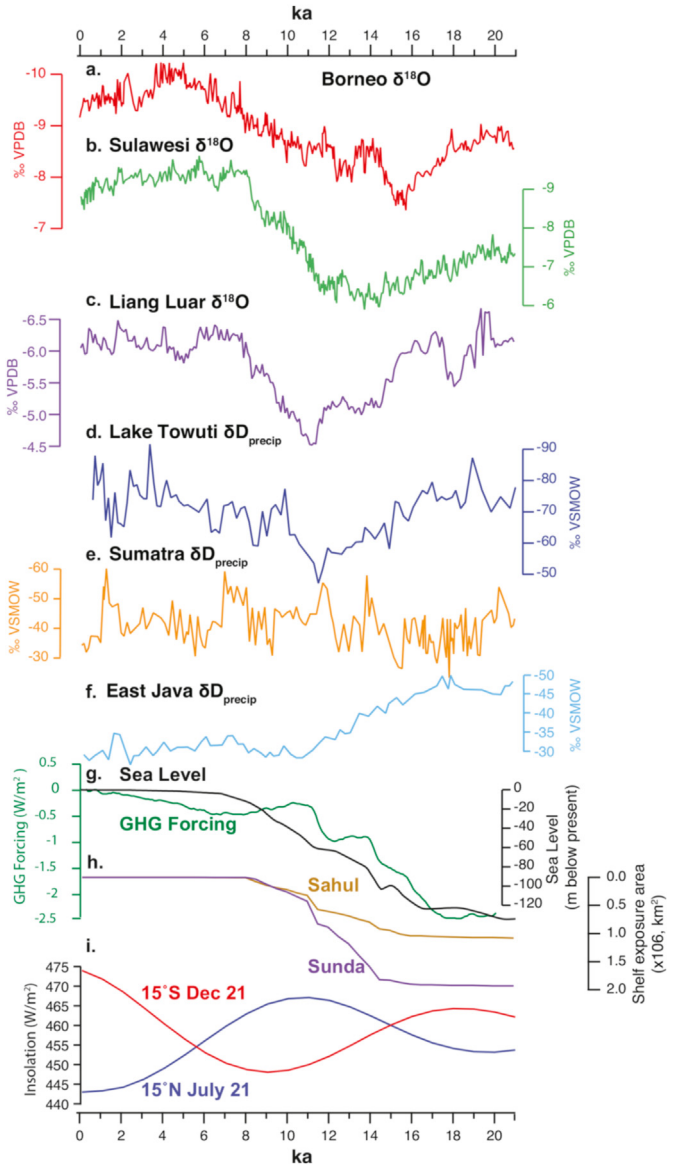

Fig. 2. (a)–(f) Selected published isotope records from the Maritime Continent and (g)–(h) potential climate forcings since the Last Glacial Maximum. (a) Speleothem $\delta^{18}O$ from Borneo (Partin et al., 2007). (b) Speleothem $\delta^{18}O$ from Sulawesi (Krause et al., 2019). (c) Speleothem $\delta^{18}O$ from Flores (Ayliffe et al., 2013). (d) Leaf wax δD from Lake Towuti (Konecky et al., 2016). (e) Leaf wax δD from northwest Sumatra (Niedermeyer et al., 2014). (f) Leaf wax δD from east Java (Ruan et al., 2019). (g) Sea level reconstruction (Lambeck et al., 2014) and radiative forcing from greenhouse gases (Schilt et al., 2010). (h) Continental shelf exposure area calculated from glacial isostatic adjustment simulations for Sahul and Sunda shelves, respectively (Pico et al., 2020). (i) December 21 insolation at 15° S, and July 21 insolation at 15° N. According to the "amount effect", more depleted isotope values correspond to wetter condition and vice versa. Note all $\delta^{18}O$ and δD_{precip} values have been corrected for changes due to global ice volume.

the IPWP during the last deglaciation (20 ka-11 ka) in response to climate forcings in the isotope-enabled Transient Climate Evolution (iTRACE) experiment and diagnose their responses to sea level and ice sheet, GHGs, orbital, and meltwater forcings. iTRACE is the first fully coupled, stable water isotope-enabled transient simulation of the last deglaciation, and we use these simulations to assess potential responses of precipitation, $\delta^{18}O_{precip}$, and δD_{precip} to deglacial climate forcings. We do not present a full data-model comparison, which will be the subject of a future paper, but this work nevertheless reveals the implications of precipitation isotope records and therefore provides a potential framework for interpreting these records over the IPWP.

2. Model simulations

iTRACE is the first transient simulation of the evolution of global climate and water isotopes during the last deglaciation (He et al., 2021). iTRACE is conducted with the isotope-enabled Community Earth System Model version 1.3 (iCESM) (Brady et al., 2019), which is composed of Community Atmosphere Model version 1.3 (CAM5.3), the Community Land Model version 4 (CLM4), Parallel Ocean Program version 2 (POP2), and Los Alamos Sea Ice Model, version 4 (CICE4). The model simulated the $\delta^{18}O_{precip}$, which we convert to δD_{precip} assuming the present-day meteoric water line. The precipitation and water isotope simulations of iCESM have been validated against modern observations at a global scale (Brady et al., 2019; Nusbaumer et al., 2017; Wong et al., 2017). A comparison of the simulations with precipitation and precipitation isotope observations across the MC suggests iCESM successfully capture the large-scale features of precipitation and water isotopes in this region, particularly changes associated with seasonal shifts of the monsoon and intertropical convergence zone (Fig. S1 and S2). CESM also realistically simulates LGM precipitation and SST in the IPWP (Zhu et al., 2017; DiNezio et al., 2018; Thirumalai et al., 2019), and therefore provides a unique opportunity for studying glacial-interglacial water isotopes and hydroclimate changes.

The simulations start from the LGM (20ka) and end at early Holocene (11ka). Four forcing factors (ICE, ORB, GHG, and MWF) are applied additively, allowing us to approximate the effect of single forcings by comparing different simulations. Continental ice sheet configuration follows the ICE-6G reconstruction (Peltier et al., 2015) and was modified every 1000 year; GHGs concentrations (CO_2, CH_4, N_2O) were prescribed based on ice-core reconstructions (Lüthi et al., 2008; Petit et al., 1999; Schilt et al., 2010); meltwater flux is approximately consistent with sea level reconstructions and follows the scheme used in TRACE-21ka (Liu et al., 2009) (see He et al., 2021 for details of forcings). The baseline simulation is integrated with changing ice sheets and ocean bathymetry (ICE). Orbital forcing was additively applied (ICE + ORB), followed by greenhouse gas (ICE + ORB + GHG). Meltwater fluxes were introduced to generate a full forcing simulation (ICE + ORB + GHG + MWF). The simulated responses to these forcings are not linearly additive, but the effect of single forcings can be approximated by subtracting the sensitivity experiments from each other as follows: the ice sheet and bathymetric effect (ICE simulation), the orbital effect (ICE + ORB simulation − ICE simulation), the GHG effect (ICE + ORB + GHG simulation − ICE + ORB simulation), and the meltwater effect (iTRACE − ICE + ORB + GHG simulation).

The ocean bathymetry was changed at 14 ka and 12 ka based on the global sea level changes implied by the ICE-6G model (Peltier et al., 2015) applied to the present-day sea-floor topography (Fig. 3). At 14 ka, the NW Australia shelf was inundated (Fig. 3b and e), as was the North Sea, Barents Sea and Kara Sea (Hughes et al., 2016). At 12 ka, the Sunda and Sahul shelves, which are shallower than the NW Australian shelf (Liu et al., 2016; Sathiamurthy and Voris, 2006) were inundated (Fig. 3c and f), and the Bering Strait was partly opened (Fig. 3c and d). To test the climate response to individual changes in ice sheet and bathymetry, sensitivity experiments were performed at 14ka and 12ka in which the ice sheet and bathymetry were changed separately. In iTRACE, the exposed Sunda and Sahul shelves are covered by a mix of C_3 grass and tropical forest.

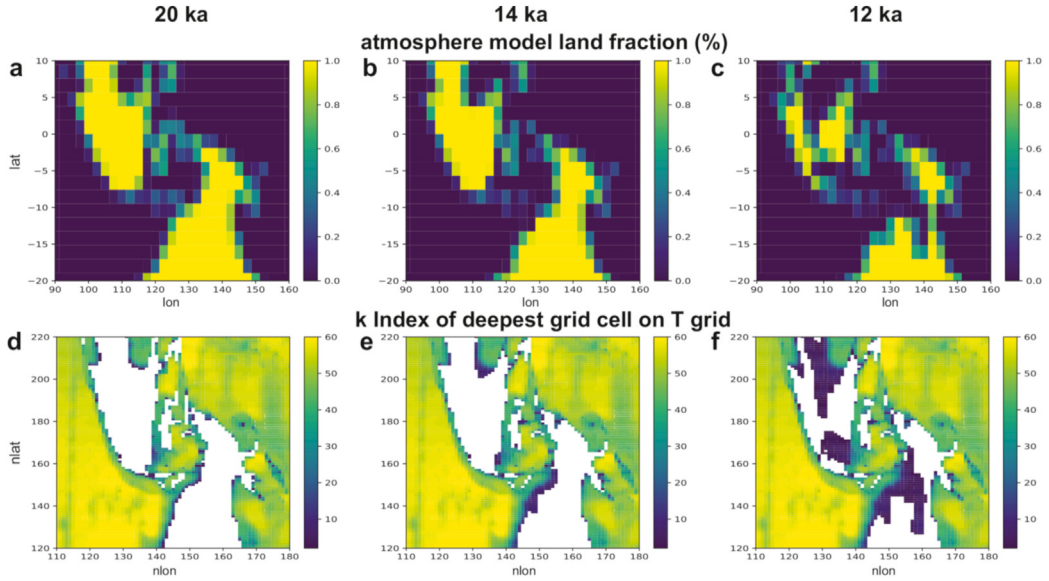

Fig. 3. Model boundary conditions representing the sea level changes during the last deglaciation in iTRACE. Atmosphere model land fraction used at (a) 20 ka, (b) 14 ka, and (c) 12 ka. Ocean model bathymetry used at (d) 20 ka, (e) 14 ka, and (f) 12 ka. K index of deepest grid cells on T grid = 0 indicates surface land points.

3. Results and discussion

3.1. Changes in precipitation and isotopic compositions during the last deglaciation

Simulated changes in mean annual precipitation during the last deglaciation (20 ka minus 11 ka anomalies) exhibit generally dry conditions over the MC, especially off the coast of Sumatra and Java, Sunda and Sahul shelves (Fig. 4a). However, the deglacial changes (20 ka minus 11 ka) in simulated annual δD_{precip} exhibit a large-scale SW-NE dipole structure: D-enriched precipitation is concentrated over the eastern IO, including Sumatra, Java, and Flores, whereas the western Pacific received D-depleted rainfall, especially in Papua New Guinea, the Sahul Shelf, North Australia, and westward to the Sunda Shelf (Fig. 4b). These distinct spatial patterns in the simulated deglacial mean annual precipitation and its isotopic composition changes were also observed from Empirical Orthogonal Function (EOF) analysis. The leading PC (PC1) of the mean annual precipitation explains 42.5% of the total variance (Fig. 5a) and its spatial pattern largely resembles that of the 20–11 ka precipitation anomalies (Fig. 4a). Regions with positive loading on PC1 are concentrated over the tropical eastern Indian and Sunda shelf, and extend eastward to western Borneo, Northern Sulawesi, and Papua New Guinea (Fig. 5a). The time series of PC1 scores indicates that generally dry conditions over the MC during the LGM were followed by a gradual transition towards wetter conditions before two-step abrupt shifts toward wetter conditions occurred around 14ka and 12ka (Fig. 5b). Meanwhile, the western equatorial

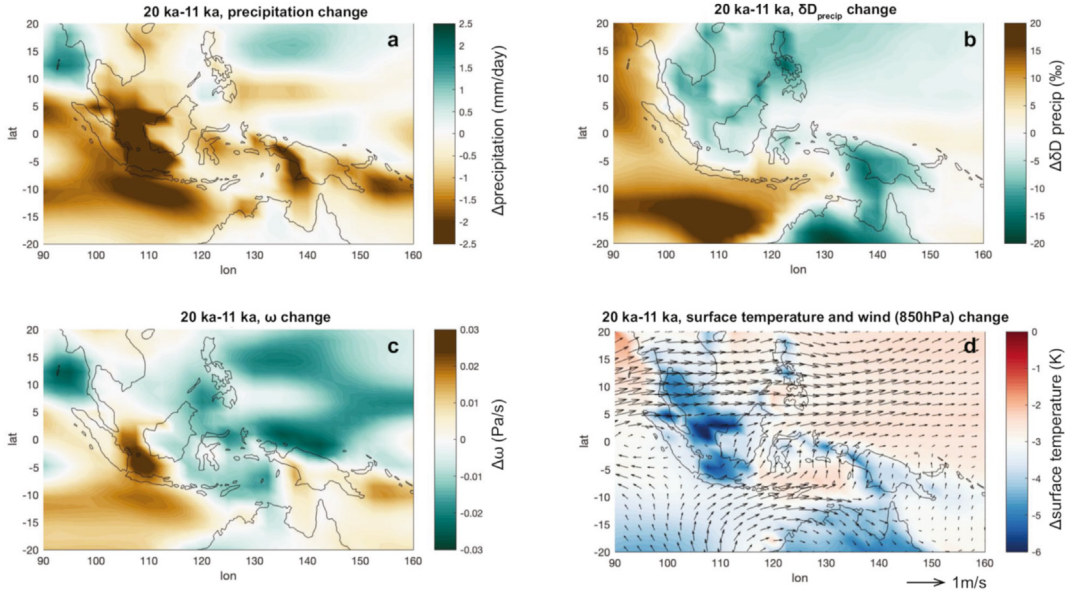

Fig. 4. Simulated changes of annual (a) precipitation, (b) δD_{precip}, (c) w (vertical velocity) at 500 hPa level, and (d) surface temperature and surface winds at 850 hPa level from 20 ka to 11 ka (20 ka minus 11 ka) in iTRACE.

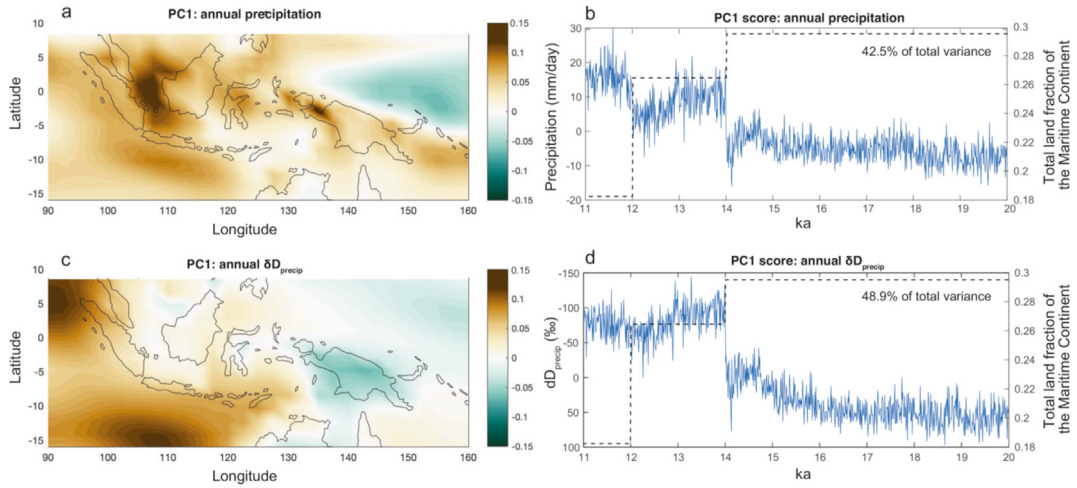

Fig. 5. Principal component analysis of annual δD_{precip} and annual precipitation from 20 ka to 11 ka in iTRACE. (a) The loading pattern and (b) time series of the first PC of annual precipitation. (c) and (d) same as (a) and (b) expect for annual δD_{precip}. The black dashed lines in (b) and (d) show the total land fraction in the Maritime Continent in iTRACE change at 14 ka and 12 ka.

Pacific side of the IPWP loads negatively on PC1, indicating a general drying trend during the last deglaciation. Regardless, the simulations predict the MC becomes wetter during the deglaciation. Again, however, the PC1 of the decadal mean annual δD_{precip} (explains 48.9% of the total variance) shows a SW-NE spatial pattern similar to that of the δD_{precip} anomalies during the last deglaciation (Fig. 5c), with positive loading over the eastern IO and widespread negative loading over the western Pacific. Regions with positive loadings are characterized by D-enriched precipitation 20 ka−16 ka, followed by a gradual trend between 16 ka and 14 ka, and an abrupt transition to more D-depletion about 14 ka (Fig. 5d). The temporal evolution and EOF pattern of the simulated D_{precip} is generally consistent with that of the proxy records over the MC region (Fig. S3).

The large-scale SW-NE dipole structure in the δD_{precip} anomalies (Fig. 4b) is associated with increased moisture convergence over the western Pacific and anomalous divergence in the eastern IO, as indicated by the vertical velocity (ω) anomalies in Fig. 4c. Converging moisture tends to be more D-depleted due to the rainout of heavy isotopes along the moisture trajectories (Galewsky et al., 2016; Konecky et al., 2019), whereas in divergence regions, the drier climate favors rain re-evaporation that removes lighter isotopes and therefore causes D-enriched precipitation. Taken together, the simulated precipitation enrichment over the eastern IO could be associated with the regional divergence anomalies indicated by increased subsidence (more positive ω), while the depleted precipitation over the north equatorial western Pacific is likely related to the regional increased moisture convergence revealed by negative ω anomalies.

In addition, the distinct EOF patterns (Fig. 5) and deglacial anomalies (Fig. 4) of the simulated mean annual δD_{precip} and precipitation indicate that the precipitation isotopes in the IPWP during the last deglaciation are influenced by processes other than local precipitation amount effects, and that the mechanisms controlling isotopic change could be location-dependent. Modern observations have demonstrated that precipitation isotopes in the IPWP can be influenced by a variety of processes including rainfall amount, moisture sources, and regional convection (Cobb et al., 2007; Moerman et al., 2013; Wurtzel et al., 2018). These processes can lead to locally and temporally variable relationships between $\delta^{18}O_{precip}$ and local precipitation amount during some seasons, and/or stronger correlation between precipitation and its isotopic composition across broader time and spatial scales (regional amount effect) (Aggarwal et al., 2016; Fudeyasu et al., 2011; Konecky et al., 2019). Modern precipitation isotopes in northwest Sumatra are strongly affected by moisture originating from the eastern IO (Wurtzel et al., 2018) (Belgaman et al., 2017). In our simulations, the δD_{precip} enrichment during the LGM over the eastern IO (Fig. 4b) is accompanied by anomalously dry condition (Fig. 4a), reduced ascension (more positive ω, Fig. 4c), and anomalous equatorial westerlies, indicating reduced convection and consequent reduced precipitation could contribute to more enriched δD_{precip} in this region, following the classic amount effect relationship. On the other hand, the δD_{precip} enrichment in southern MC around Savu Sea could be associated with the more D-enriched moisture source from the eastern IO delivered by southwesterly winds.

Conversely, in the present-day climate of northern Borneo and northwest Sumatra, moisture sources shift between the South China Sea (boreal winter) and Java Sea (boreal summer) associated with latitudinal movement of the ITCZ (Moerman et al., 2013), yet regional convective activity and precipitation amount (regional amount effect) is thought to explain rainfall isotope variability on longer time scales (Cobb et al., 2007; Moerman et al., 2013; Wurtzel et al., 2018). In our simulations, anomalously dry conditions (Fig. 4a), cooling (Fig. 4d) and increased subsidence indicated by more positive ω change are observed over Sunda and Sahul Shelves, but the corresponding δD_{precip} is more depleted in these regions (contrary to the amount effect) suggesting processes associated with shelf exposure contribute to the δD_{precip} depletion (discussed in detail in Section 3.3). These processes also affect the simulated $\delta^{18}O_{precip}$, and δD_{precip} on adjacent islands such as Borneo.

Precipitation variations in southern and central MC in the present day are largely controlled by the Australian-Indonesian monsoon (Belgaman et al., 2017; Griffiths et al., 2009), and exhibit more depleted precipitation isotopes in the wet season (December to May) and more enriched isotopic signal in dry season (June to November) (Belgaman et al., 2017; Griffiths et al., 2009). In the iTRACE simulations, D-enrichment in the southern MC generally does correspond to lower precipitation amounts. However, the Australian-Indonesian summer monsoon was intensified during the LGM, indicated by the anomalous northwesterlies during DJF over the central IPWP (Fig. S4). The intensified Australian-Indonesian summer monsoon circulation, combined with

stronger moisture convergence in the central MC (indicated by more negative ω) appears to drive D-depleted precipitation in this region during the LGM despite lower precipitation amounts (Fig. S4), as suggested by Konecky et al. (2016). On the other hand, the D-depleted rainfall over the west Pacific (north of Papua and east of Sunda Shelf) could be associated with regional increases in moisture convergence indicated by more negative ω (Fig. 4c). Thus, the simulations suggest highly variable relationships between precipitation amounts and isotopic compositions, with (regionally) strong effects of shelf exposure on these relationships.

3.2. Response to climate forcings

In the ICE + ORB + GHG simulation, the precipitation and isotope changes across the tropical domain exhibits a strong dipole patterns across the IO. The amplitude of precipitation changes is particularly strong over the MC relative to other tropical regions, and the strong zonal gradients that develop over the IO stands in contrast to more meridional patterns observed over the tropical Atlantic and Pacific (Fig. 6). These features suggest either unique simulated responses of MC precipitation to global climate forcings during the last deglaciation, or strong regional responses to unique regional forcings – likely responses to MC shelf exposure (e.g. DiNezio et al., 2018). To further explore this question, we calculated the precipitation and δD_{precip} anomalies at 20 ka relative to 11 ka (20 ka minus 11 ka) in ICE, GHG, and ORB simulations, respectively (Fig. 7). MW also contributed to the precipitation and δD_{precip} anomalies during the last deglaciation, but the difference in meltwater flux forcing and associated strength of AMOC at 20 ka and 11ka is relatively small, so the corresponding response is not discussed in detail in this section.

The ICE simulation (Fig. 7c and d) exhibits a similar spatial pattern of precipitation and δD_{precip} anomalies to the full forcing simulation (Fig. 7a and b), with aridity and δD_{precip} enrichment over the eastern IO, and depletion with wetter condition over the western Pacific. The influence of GHG and ORB forcings is weaker (Fig. 7e–h), and both simulate wet conditions in the tropical eastern IO, in contrast to the dry conditions in the ICE and ICE + ORB + GHG simulations. This suggests that the forcings in the ICE simulations primarily explain the simulated deglacial precipitation and δD_{precip} variations across the IPWP. As in the full forcing experiments, the precipitation isotopic compositions in response to single forcing also exhibit regionally variable changes that, in many cases, do not follow the local "amount effect".

GHG forcing leads to modest precipitation change over the MC, whereas wetter and drier conditions dominate the eastern IO and western Pacific, respectively (Fig. 7e). The Walker circulation over the IO strengthened in response to lower GHGs during the LGM, evidenced by westerly anomalies along the equatorial IO and cooler western IO relatively to the eastern IO (Fig. S5d). Stronger

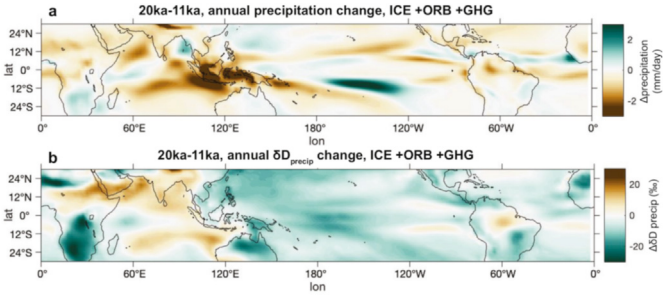

Fig. 6. Simulated precipitation (a) and δD_{precip} (b) changes in ICE + ORB + GHG simulation across the tropical domain.

ascending motion (more negative ω, Fig. S5c) over the eastern IO explains the wetter conditions with more depleted δD_{precip} over the eastern IO, whereas enhanced subsidence (more positive ω, Fig. S5c) occurs alongside drying and δD_{precip} enrichment over the western IO and equatorial East Africa (Fig. S5a). This response to lower GHGs is consistent with previous simulations, which show anomalous westerlies along the equatorial IO, accompanied by suppressed equatorial upwelling and deeper thermocline in the east IO during the LGM (Otto-Bliesner et al., 2014; DiNezio et al., 2018). The stronger IO Walker circulation at 20 ka could also be associated with northerly wind anomalies in the northwestern IO caused by an enhanced Mediterranean/Arabian anticyclone, as seen in previous simulations (Otto-Bliesner et al., 2014). In the TraCE-21 simulation used by Otto-Bliesner at al. (2014), continental cooling in North Africa and the Arabian Peninsula in response to lower GHG concentrations intensifies the Mediterranean/Arabian anticyclone. The consequent northerly wind anomalies advect cool/dry air to the western IO, and the reduced SST over the western IO increases the zonal SST gradient across the IO, contributing to a stronger IO Walker circulation (Fig. S5). While this mechanism appears to operate in our simulations, only modest precipitation change was simulated over the tropical eastern IO in response to GHG forcing (Fig. 7e and S5a). This small response might be due to decreased atmospheric moisture content in the simulation (indicated by reduced specific humidity in Fig. S5e) in response to colder surface temperature at LGM (following the Clausius-Clapeyron relationship), which partially compensated for the influence of strengthened ascending motion over this region, as suggested by Cao et al. (2019). Additionally, the enhanced regional deep convection (more negative ω) over the MC caused by strengthened Walker circulation, combined with reduced specific humidity should contribute to more depleted δD_{precip} (Fig. S5b-2e) despite slightly drier conditions (Fig. S5a). On the other hand, the precipitation reduction and δD_{precip} enrichment observed over the equatorial western Pacific Ocean (150–180°E, Fig. 7e, Fig. S5a and S5c) is consistent with the anomalous subsidence indicated by anomalous easterly wind and more positive ω over the western equatorial Pacific (Fig. S5a and S5c).

The ORB forcing contributes to a meridional precipitation gradient over the MC. Sumatra, Borneo, and northern Sulawesi were dominated by drying, whereas wet conditions developed over the southeastern IO extending to Java and Flores (Fig. 7g and h). The spatial pattern of δD_{precip} anomalies in response to ORB forcing were generally consistent with that of precipitation, following the amount effect, except for δD_{precip} enrichment in the northeastern IO and slightly depleted δD_{precip} in southern Borneo and Sulawesi. The anomalous NH summer cooling at LGM driven by precessional forcing is expected to weaken the ascending branch of the SH Hadley cell and cross-equatorial winds (McGee et al., 2014). Meanwhile, the reduced NH summer ocean-continent temperature gradient during the LGM tends to weaken the Asian summer monsoon (Cheng et al., 2012). These changes would contribute to decreased summer (JJA) precipitation in the northern MC, including Borneo, Sumatra, and Sulawesi (Fig. 7g, S6). However, in our simulations, ORB forcing produces zonal precipitation and precipitation isotope changes as well. The weakened SH Hadley cell across the equatorial Indo-Pacific Ocean leads to a northwesterly anomaly over the equatorial Indo-Pacific Ocean (Fig. S6c-3d), which together with the zonal surface temperature gradient (warmer western IO and cooler eastern IO), indicates stronger Walker circulation along the equatorial IO (Fig. S6). This explains the wetter conditions observed over the southeastern IO off Java. This response to orbital forcing is also supported by the opposite atmospheric responses (strengthened southeasterly over the equatorial Indo-Pacific Ocean and stronger Asian summer monsoon) simulated for the mid-

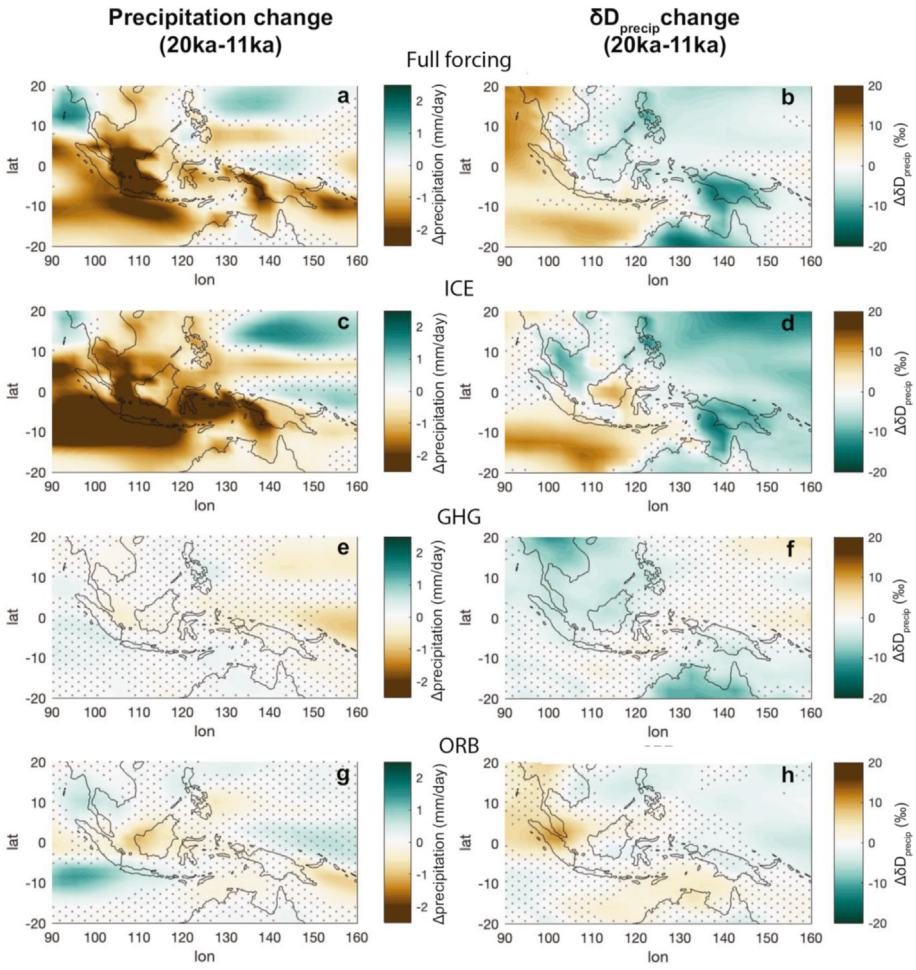

Fig. 7. Changes of annual precipitation (left) and annual δD_{precip} (right) from 20 ka to 10 ka (20 ka minus 11 ka) in (a–b) fullforcing run, (c–d) ICE run, (e–f) GHG effect, and (g–h) ORB effect. Differences insignificant at the 95% confidence level according to the Student's *t*-test are dotted.

Holocene, when NH summer insolation increased (Bosmans et al., 2012; Tian et al., 2018).

This analysis demonstrates that both GHGs and ORB forcing contribute to a stronger Walker circulation along the equatorial IO during the LGM relative to the early Holocene, resulting in a wetter eastern IO and drying in the western IO. However, these responses are opposite to the dry conditions over the eastern equatorial IO and MC apparent in the ICE simulation, which further appears to dominate the responses in the full-forcing simulation (Fig. 7a–d). This result indicates that sea level and/or ice sheet changes mainly control the changes in precipitation and isotopic responses across the IO in the iTRACE simulation.

3.3. The influence of shelf exposure

The ICE experiment in iTRACE integrated changes in ice sheets and sea level, both of which could affect hydroclimate changes over the MC during the deglaciation. A number of previous studies have suggested changes in land-sea configuration due to sea level fluctuation as the main control on the glacial-interglacial precipitation changes across the IO (DiNezio et al., 2011, 2018; DiNezio and Tierney, 2013; Windler et al., 2019, 2020). DiNezio et al. (2013, 2016, 2018) proposed that the exposure of Sahul Shelf due to lower LGM sea level excited a positive ocean-atmosphere feedback along the equatorial Indian Ocean, involving a stronger surface temperature gradient and a weaker Walker circulation, which was responsible for the drier western IO and wetter eastern IO dipole pattern. Changes in ice sheet albedo/topography during the LGM have also been reported to impact tropical hydroclimate changes by modulating the intensity of the Indian monsoon (DiNezio et al., 2018) and influencing the latitudinal position of ITCZ and strength of Hadley cell (Lee et al., 2015), respectively. It remains unclear whether proxy reconstructions fully support these simulations, as the timing (e.g. Russell et al., 2014) and sign (e.g. Mohtadi et al., 2017) of reconstructed hydroclimate changes in many records contradicts these simulations. Here we examine the mechanisms and isotopic signals associated with ICE and ocean bathymetric changes to help guide future reconstructions and data-model comparisons.

The global mean sea level rises by approximately 80 m between the LGM and 11 ka due to the decay of ice sheets (Clark et al., 2012). The relatively low sea level at LGM exposed the Sunda Shelf, currently located underneath the Gulf of Thailand, the South China Sea, and Java Sea, as well as the Sahul Shelf, the continental shelf extending from the northwestern coast of Australia to the island of New Guinea underneath the Gulf of Carpentaria and the Timor Sea (Fig. 1). In iTRACE, the sum of land fraction in the MC (16°S-8°N, 90°E-160°E) decreased modestly from 30% to 26% from LGM to 14 ka (Fig. 3b and e), and dropped again to 18% at 12ka (Fig. 3c and f). At 14ka, seawater inundated the NW Australian Shelf, which presently has depth exceeding 65 m, whereas the main parts of Sunda and Sahul shelves remained exposed until their submergence after

12ka (Fig. 3). In contrast, topography of ice sheets was modified every 1000 years, following the ICE-6G configurations.

The leading PCs of precipitation and δD_{precip} exhibit a pronounced shift at 14 ka (Fig. 5c and d). These results alongside the similarity of the spatial responses in the ICE and full-forcing experiments suggest sea level change and associated shelf exposure are the first order control of the simulated precipitation and isotopic composition changes in the MC. However, continental ice sheets in ICE simulation were also modified at 14 ka, and tropical precipitation may exhibit highly non-linear responses to ice sheet configuration (Lee et al., 2015). To test the contribution of shelf exposure at this time, we analyzed a sensitivity experiment with ocean bathymetry and ice sheet changed separately at 14 ka (Fig. S8). The response of precipitation, surface temperature, and wind stress to bathymetry change (Fig. S8c) strongly resemble the climate anomalies across 14 ka in the ICE simulation (Fig. S8b). Meanwhile, the climate response to ice sheet change (Fig. S8d) is much weaker and no clear spatial pattern of precipitation was observed across the IO. In addition, a short-lived reduction in AMOC was observed at 14 ka in ICE run; however, analyses of the precipitation changes over the IO indicate that the precipitation anomalies persist long after the AMOC largely recovered (Fig. S9). This sensitivity experiment therefore confirms shelf exposure as the first order control of changing precipitation patterns across the Indian basin during the deglaciation in these simulations.

The simulated precipitation changes at 14 ka exhibit a large-scale dipole across the entire IO, characterized by wetter conditions over the western IO and drier conditions over the eastern IO (Fig. 8a). The spatial pattern of the δD_{precip} anomaly generally resembles that of precipitation anomalies and follows the classic amount effect, with enrichment in the southeastern IO, northern Australia, and the MC, except for Papua New Guinea (Fig. 8b). The changes in annual surface temperature also exhibit a dipole pattern across the Indian basin: warmer conditions were observed over the western IO while eastern IO and the MC is cooler (Fig. 8c). Anomalous easterly wind along the equatorial IO is consistent with the anomalies in surface temperature and precipitation. Increased convection and anomalous ascending motion over the warmer SSTs lead to increased precipitation over the western IO, whereas anomalous descending motion and surface wind divergence over the cooler eastern IO contribute to the dry condition in this region. A generally similar but geographically smaller and weaker dipole pattern developed at 12 ka with the second stage of shelf inundation in the simulations. We note that the abruptness of these changes at 14 and 12 ka are unrealistic, due to the instantaneous inundation of the shelves in the simulations. Nevertheless, these results imply that in this model shelf exposure triggers strong ocean-atmosphere interactions consistent with a Bjerknes feedback over the Indian Ocean that weakens the Walker Circulation, creating dipole anomalies in precipitation amount and isotopic compositions.

Previous model simulations and proxy reconstruction studies also suggest that shelf exposure is the main driver of IPWP hydroclimate during the LGM (Di Nezio et al., 2016; DiNezio et al., 2018; Windler et al., 2020). Di Nezio et al. (2016) diagnosed the influence of Sahul and Sunda Shelves separately using a series of simulations with CESM1, and concluded that Sahul Shelf exposure is the main driver of the IO hydroclimate dipole at LGM. In those simulations, the surface cooling of the exposed Sahul reduced atmospheric convection, which is then amplified by air-sea interactions over the IO. This result is generally consistent with our explanation for the hydroclimate anomalies across 14 ka observed in iTRACE, except that in iTRACE only the NW Australian shelf (which is part of the Sahul Shelf in the experiments of Di Nezio et al., 2016) was submerged across 14 ka. The positive Bjerknes feedback we observe before 14 ka appears to be triggered by an anomalous southeasterly wind off the coast of Sumatra and Java, which would induce the upwelling of cold subsurface water in the region. The shallower thermocline in the eastern IO and strengthened zonal SST gradient would further contribute to anomalous easterly winds along the IO and amplify the initial response. The southeasterly anomalies appear to be associated with the exposure of the NW Australia shelf, potentially due to land-sea gradients that arise from surface cooling over the exposed shelf. This result suggests the NW Australian shelf, rather than the Arafura Shelf (eastern Sahul Shelf) plays a critical role in inducing the easterly anomalies and coastal upwelling off Sumatra. Additionally, the pattern of warm/wet western IO and cool/dry eastern IO peaks during SON (Fig. S7), when the easterly wind anomaly is amplified by Bjerknes feedback (e.g. Di Nezio et al., 2016). Thus, we conclude that exposure of the NW Australia shelf activates the Bjerknes feedback across the IO, which triggers large dipolar changes in simulated precipitation and δD_{precip} arises in this region.

The main body of Sunda and Sahul shelves became submerged after 12 ka in iTRACE, and although this triggers further dipole responses in precipitation and precipitation isotopes over the IO, the corresponding hydroclimate changes are much weaker and are mainly centered over the now submerged shelf regions. This is distinct from the cross-equatorial IO response to the exposure of NW Australia shelf prior to 14 ka (Fig. 8). Before 12ka, precipitation and surface temperature over Sunda and Sahul shelves decreased dramatically, accompanied by more depleted δD_{precip}. Anomalous

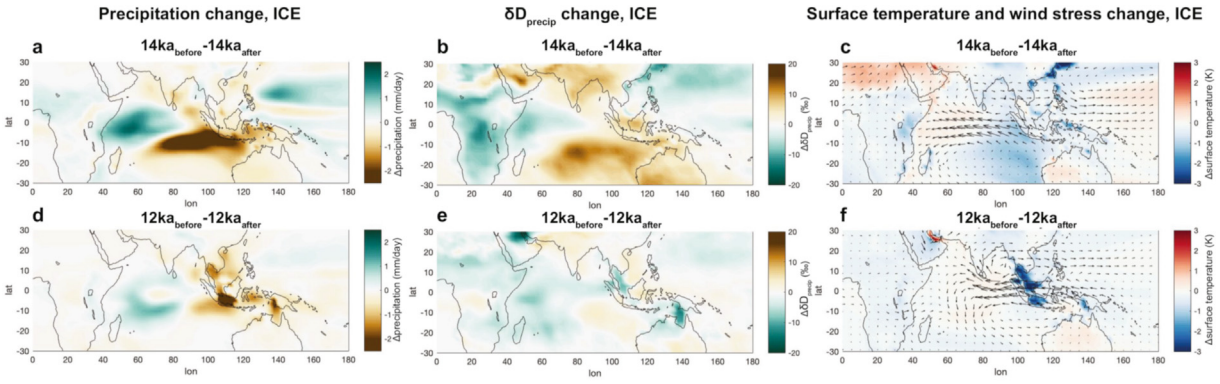

Fig. 8. Simulated climatic response to shelf exposure effect before 14 ka and 12 ka. Changes of annual (a) precipitation, (b) δD_{precip}, and (c) surface temperature and winds (at 850 hPa level) before and after 14 ka (100-year mean before 14 ka minus 100-year mean after 14 ka) in ICE run. (d)–(f) same as (a)–(c) except for changes before and after 12 ka (100-year mean before 12 ka minus 100-year mean after 12 ka).

easterly wind was observed over the Sunda shelf and the eastern equatorial IO, and cooling of the exposed shelves reduced the convection, weakening the precipitation over the shelves (Fig. 8d–f). In addition, water vapor concentrations are lowered by the increase in land area, leading to more depleted δD_{precip} over the exposed Sunda and Sahul shelves despite decreased precipitation. The weak precipitation and surface temperature dipole along the equatorial IO indicate that, associated with the exposure, the positive IO Bjerknes feedback is only weakly excited, resulting in relatively weaker and more localized hydroclimate response. This result is consistent with that of Di Nezio et al. (2016) who found that the Sunda Shelf exposure is unable to excite the IO Bjerknes feedback because of the location and seasonality of the corresponding upwelling. SSTs are more sensitive to changes in the thermocline depth where upwelling is strong (Li et al., 2003). The easterly anomalies caused by the exposed Sunda Shelf are located over the NE IO, where the coastal upwelling is relatively weak compared to that off the coast of Sumatra and east Java. Additionally, the strength of easterly anomalies peaked in DJF, when coastal downwelling prevails. This mechanism could explain why in iTRACE, hydroclimate response to the submergence of the Sunda and Arafura Shelves at 12 ka is more localized, compared to the large-scale response to the NW Australia shelf exposure before 14 ka.

In sum, our analyses suggest that exposure of the NW Australian shelf leads to strong, coupled ocean-atmospheric circulation changes that result in a precipitation amount and isotope anomalies over the Indian Ocean during the LGM. The subsequent inundation of the Sunda and eastern Sahul shelves lead to climate anomalies localized over the exposed land areas, with drying and D-depleted precipitation during the LGM. This, in turn, has important implications for the timing of precipitation, δD_{precip}, and $\delta^{18}O_{precip}$ changes in proxy records, due to the differences in water depth and the timing of inundation of the NW Australian versus the Sunda and Arafura shelves.

3.4. Diverse regional sensitivities to shelf exposure and climate forcings

Our results show location-dependent relationships between changes in precipitation amount and isotopic composition, as well as heterogeneous responses to different forcings across the MC during the LGM and deglaciation. Previous work has documented large precipitation isotopic differences in proxy records (e.g. speleothem $\delta^{18}O$ and leaf wax δD) over short spatial scales in the MC (e.g. across Sulawesi) during the last deglaciation (Konecky et al., 2016; Krause et al., 2019; Wicaksono et al., 2017). However, compilations of geological and paleocological data suggests a more uniform LGM drying (DiNezio and Tierney, 2013; DiNezio et al., 2018). Some isotopic records suggest “time-varying” controls on the precipitation isotopic composition. For example, anti-correlation between δD_{wax} and $\delta^{13}C_{wax}$ was reported from Mandar Bay and central Sulawesi during the last deglaciation, indicating the influence of non-amount effects, whereas positive correlation consistent with the amount effects was found after the shelf submergence (Konecky et al., 2016; Wicaksono et al., 2017). Although a more direct proxy-model comparison is required to fully explain these reconstructions, our results suggest that variable regional sensitivities to different climate forcings, and shelf exposure in particular, combined with opposing effects from orbital and greenhouse gas forcing, can produce spatiotemporally heterogeneous precipitation and isotopic correlations and changes in the MC.

Current sea level reconstructions combined with the modern ocean bathymetry suggest the NW Australian shelf (water depth over which ranges from −110 to −65 m) was inundated between 15.6 and 12.5 ka (Fig. S11), preceding inundation of the shallower Sunda and Arafura shelves. Despite the strong influence of NW Australian shelf exposure on precipitation and δD_{precip} in our simulations, it is unclear whether the responses observed in proxy reconstructions match our simulated changes. It is possible that our simulation overestimates the influence of shelf exposure, which could complicate evaluation of the precipitation and isotopic responses in proxy records given the generally opposing influences from other forcings (GHG and ORB). Indeed, other LGM simulations (e.g. CCSM3) show different climate patterns during the LGM over the IO (Mohtadi et al., 2017) compared to iTRACE. A more detailed analysis of spatial patterns of proxy data is needed to test the simulation results, particularly considering the large differences over short spatial scales in our simulations and that the model may ‘misplace’ the boundaries between these responses.

In iTRACE, the NW Australian shelf exposure induces southeasterly anomalies off the coast of southern Sumatra and Java. The consequent stronger upwelling activates an IO Bjerknes feedback and leads to a precipitation dipole along the equatorial IO. Remarkable changes in precipitation and isotopic composition are simulated off the coast of southern Sumatra and Java, as shown in Fig. 9b and e: precipitation in these two regions reduced significantly before 14 ka (when NW Australian shelf was exposed), accompanied by more enriched precipitation isotopes. A more moderate decrease in precipitation was observed before 12 ka due to anomalous subsidence and decreased atmospheric convection caused by the emergence of the Sunda Shelf, accompanied by δD_{precip} enrichment. Dry condition, and δD_{precip} enrichment were indeed observed in proxy records from marine sediments off southern Sumatra during glacial periods, attributed to the exposure of Sahul and Sunda shelves (Windler et al., 2019, 2020). In contrast, increased thermocline depth recorded off Sumatra and southeast Java during the LGM suggests a stronger Indian Ocean Walker circulation (Mohtadi et al., 2017), indicating a potential effect of different forcings.

Our simulations suggest shelf exposure effects were very limited in northwest Sumatra, which could be due to locally opposing responses to the exposure of NW Australian and Sunda shelves (Fig. 8) as well as the influence of orbital forcing. This prediction is supported by reconstructions indicating little change in δD_{precip} in NW Sumatra from LGM to the Holocene (Niedermeyer et al., 2014). We observed little change in δD_{precip} in the simulations in east Java across 12 ka (Fig. 9e), potentially because δD_{precip} enrichment caused by weaker atmospheric convection is partially counteracted by a more depleted moisture source, as the exposed Sunda and Sahul shelves increase the distance over land that the monsoon traveled en route to East Java (Winnick et al., 2014). The resulting rainout and reduced availability of moisture from the ocean would lead to a more depleted moisture source for East Java and adjacent regions. Differences in the contributions to precipitation isotopic compositions from local precipitation amount, regional convection, and moisture source could potentially lead to the discrepancy in δD_{precip} reconstructions from East Java and Flores (Ayliffe et al., 2013; Griffiths et al., 2009; Ruan et al., 2019).

The influence of shelf exposure weakens eastward of the Sunda Shelf across the central and eastern MC in our model (Fig. 9). Simulated precipitation in eastern Sulawesi exhibits only a modest increase in response to the flooding events at 14 ka and 12 ka (Fig. 9d), and shows a gradual trend toward wetter condition due to increasing GHG throughout the last deglaciation (Fig. S10e and S10f). On the other hand, simulated δD_{precip} in eastern Sulawesi is more depleted before 14 ka, which is attributed to the more isotopically depleted air masses from the South China Sea delivered by northerly monsoon winds. Modest enrichmentment in δD_{precip}

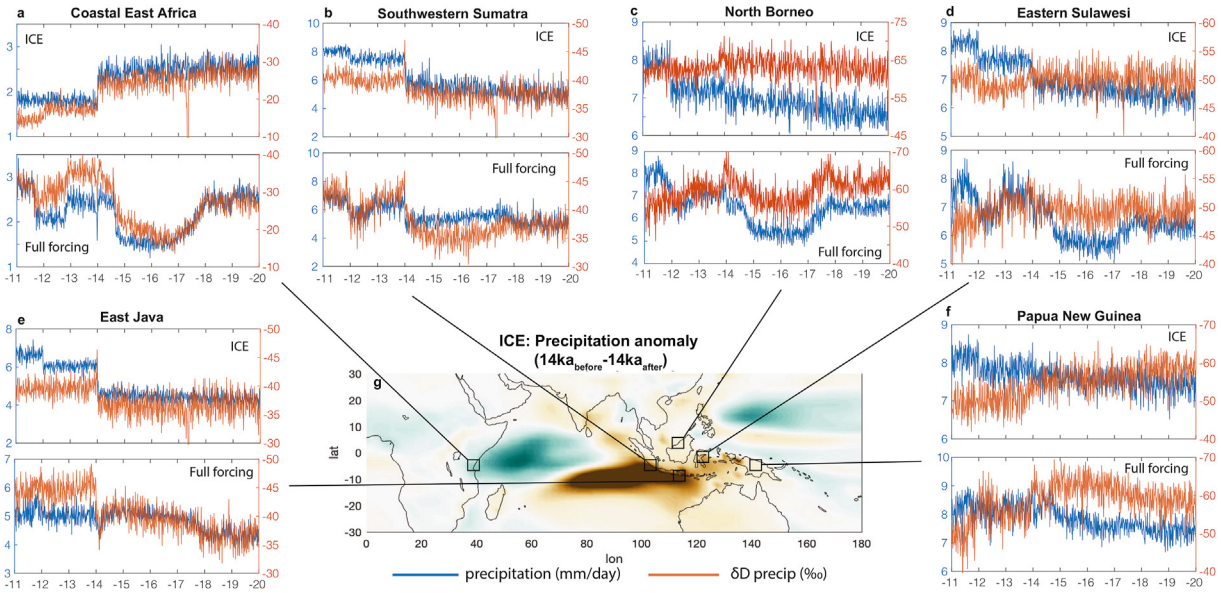

Fig. 9. Simulated precipitation and isotopic signal response to the exposure of NW Australian shelf before 14 ka from ICE run and full forcing run in (a) coastal East Africa, (b) Southwestern Sumatra, (c) North Borneo, (d) Eastern Sulawesi, (e) East Java, and (f) Papua New Guinea. (g) Precipitation anomalies before and after 14 ka in ICE run.

was found before 12 ka, likely due to anomalously reduced ascending motion associated with the surface cooling of exposed Sunda and Sahul shelves. More isotopically depleted precipitation during the LGM was also reported from Lake Towuti, which was attributed to advection of depleted moisture sources associated with intensified monsoon circulation (Konecky et al., 2016). Similar to eastern Sulawesi, decreased precipitation in response to the exposure of Sunda shelf before 12 ka is predicted in north Borneo, but no detectable response to the exposure of NW Australian shelf was found (Fig. 9c). Little response to 12 ka and 14 ka flooding events from Papua New Guinea (Fig. 9f) further suggests the limited influence of shelf exposure effect on the eastern MC.

A more detailed data-model comparison will be the subject of a future paper, but our results already highlight the complexity of the atmospheric, oceanic, and isotopic responses to orbital-scale forcings over the Maritime Continent during the LGM. This complexity stands in contrast to the meridional patterns observed in other parts of the tropics during the LGM in iTRACE (Fig. 6). Given the large land configuration changes in the MC, and the general absence of similar changes in other parts of the tropics, this difference further highlights the potential importance of shelf exposure to the simulated glacial climate of the MC.

4. Conclusion

We investigated deglacial hydroclimate and water isotope changes in the IPWP and corresponding climate forcings using an isotope-enabled Transient Climate Experiment (iTRACE). Our analysis demonstrates land-sea configuration is the dominant forcing of long-term changes in simulated precipitation and isotopic signals in IPWP during the last deglaciation. Land mass exposure within the IPWP in response to lower sea level at LGM induces a weaker Walker circulation along the equatorial IO, leading to a strong, large-scale wetter/drier dipole along the basin and an overall drying over the MC. Our simulations suggest that exposure of NW Australian shelf excited a Bjerknes feedback across the equatorial IO, and the consequent weaker Walker circulation led to a warm/wet western IO and cool/dry eastern IO and a corresponding δD dipole along the IO. In contrast, the influence of Sunda and Arafura shelves exposure (before 12 ka) is mainly constrained to the locally exposed areas, due to a much weaker atmosphere-ocean response. Sunda and Arafura Shelf exposure cause surface cooling, weakening vertical convection, and resulting in local drying. These processes are associated with more depleted precipitation isotopes over the emergent continental shelf, likely due to a combination of moisture source and circulation changes.

In the MC, the simulated influence of shelf exposure effect is strongest over the eastern IO and costal Sumatra and Java, and diminished eastward to the central and western MC. However, GHGs and orbital forcing contribute to a weak precipitation dipole across IO that partially opposes the response to Shelf exposure. In addition, location-dependent responses to GHGs and ORB forcings were also observed in the MC. Considering the complexity of these responses, the sharp regional gradients within the MC, and the opposite response to different forcings, it may be difficult to reconstruct precipitation amount in this region purely from proxies of precipitation isotopes. However, combining precipitation isotopic reconstructions with other indicators of precipitation amount may allow diagnosis of the oceanic and atmospheric circulation changes and their associated forcings in this critical region.

Author contributions

All authors made substantial contributions to this work and have approved the final version of the manuscript. X.D. analyzed the data and wrote the manuscript. J.R. supervised the project and contributed to the manuscript. Z.L. and B.L.O.-B proposed the iTRACE research and designed the experiments. C.Z., Y.G., and C.H. performed the experiments and contributed to the model development. D.O., M.M., Y.Y., and V.G. contributed to proxy interpretations. All authors contributed to discussions and the revision of the manuscript.

Declaration of competing interest

The authors declare that they have no known competing financial interests or personal relationships that could have appeared to influence the work reported in this paper.

Acknowledgements

This work was supported by the Voss Postdoctoral Fellowship at Brown University, Institute at Brown for Environment and Society, the NSF-EAR 2102856 to J. Russell, the NSF-AGS 1656907 to Z. Liu, and Deutsche Forschungsgemeinschaft (DFG) grant MO2546/3–1 to M. Mohtadi.

Appendix A. Supplementary data

Supplementary data to this article can be found online at https://doi.org/10.1016/j.quascirev.2021.107188.

References

Aggarwal, P.K., Romatschke, U., Araguas-Araguas, L., Belachew, D., Longstaffe, F.J., Berg, P., Schumacher, C., Funk, A., 2016. Proportions of convective and stratiform precipitation revealed in water isotope ratios. Nat. Geosci. 9, 624–629.

Ayliffe, L.K., Gagan, M.K., Zhao, J.-x., Drysdale, R.N., Hellstrom, J.C., Hantoro, W.S., Griffiths, M.L., Scott-Gagan, H., Pierre, E.S., Cowley, J.A., Suwargadi, B.W., 2013. Rapid interhemispheric climate links via the Australasian monsoon during the last deglaciation. Nat. Commun. 4, 2908.

Belgaman, H.A., Ichiyanagi, K., Suwarman, R., Tanoue, M., Aldrian, E., Utami, A.I., Kusumaningtyas, S.D., 2017. Characteristics of seasonal precipitation isotope variability in Indonesia. Hydrol. Res. Lett. 11, 92–98.

Boos, W.R., 2012. Thermodynamic scaling of the hydrological cycle of the last glacial Maximum. J. Clim. 25, 992–1006.

Bosmans, J.H.C., Drijfhout, S.S., Tuenter, E., Lourens, L.J., Hilgen, F.J., Weber, S.L., 2012. Monsoonal response to mid-holocene orbital forcing in a high resolution GCM. Clim. Past 8, 723–740.

Brady, E., Stevenson, S., Bailey, D., Liu, Z., Noone, D., Nusbaumer, J., Otto-Bliesner, B., Tabor, C., Tomas, R., Wong, T., Zhang, J., Zhu, J., 2019. The connected Isotopic water cycle in the community earth system model version 1. J. Adv. Model. Earth Syst. 11 (8), 2547–2566. https://doi.org/10.1029/2019MS001663.

Cao, Jian, Wang, Bin, Liu, Jian, 2019. Attribution of the last glacial maximum climate formation. Clim. Dynam. 53 (3), 1661–1679. https://doi.org/10.1007/s00382-019-04711-6.

Cheng, H., Sinha, A., Wang, X., Cruz, F.W., Edwards, R.L., 2012. The global paleomonsoon as seen through speleothem records from Asia and the Americas. Clim. Dynam. 39, 1045–1062.

Chiang, J.C.H., 2009. The tropics in paleoclimate. Annu. Rev. Earth Planet Sci. 37, 263–297.

Chiang, J.C.H., Bitz, C.M., 2005. Influence of high latitude ice cover on the marine Intertropical Convergence Zone. Clim. Dynam. 25, 477–496.

Clark, P.U., Shakun, J.D., Baker, P.A., Bartlein, P.J., Brewer, S., Brook, E., Carlson, A.E., Cheng, H., Kaufman, D.S., Liu, Z., Marchitto, T.M., Mix, A.C., Morrill, C., Otto-Bliesner, B.L., Pahnke, K., Russell, J.M., Whitlock, C., Adkins, J.F., Blois, J.L., Clark, J., Colman, S.M., Curry, W.B., Flower, B.P., He, F., Johnson, T.C., Lynch-Stieglitz, J., Markgraf, V., McManus, J., Mitrovica, J.X., Moreno, P.I., Williams, J.W., 2012. Global climate evolution during the last deglaciation. Proc. Natl. Acad. Sci. Unit. States Am. 109, E1134.

Clement, A.C., Hall, A., Broccoli, A.J., 2004. The importance of precessional signals in the tropical climate. Clim. Dynam. 22, 327–341.

Cobb, K.M., Adkins, J.F., Partin, J.W., Clark, B., 2007. Regional-scale climate influences on temporal variations of rainwater and cave dripwater oxygen isotopes in northern Borneo. Earth Planet Sci. Lett. 263, 207–220.

Dansgaard, W., 1964. Stable isotopes in precipitation. Tellus 16, 436–468.

Di Nezio, P.N., Timmermann, A., Tierney, J.E., Jin, F.-F., Otto-Bliesner, B., Rosenbloom, N., Mapes, B., Neale, R., Ivanovic, R.F., Montenegro, A., 2016. The climate response of the Indo-Pacific warm pool to glacial sea level. Paleoceanography 31, 866–894.

DiNezio, P.N., Clement, A., Vecchi, G.A., Soden, B., Broccoli, A.J., Otto-Bliesner, B.L., Braconnot, P., 2011. The response of the Walker circulation to Last Glacial Maximum forcing: implications for detection in proxies. Paleoceanography 26.

DiNezio, P.N., Tierney, J.E., 2013. The effect of sea level on glacial Indo-Pacific climate. Nat. Geosci. 6, 485–491.

DiNezio, P.N., Tierney, J.E., Otto-Bliesner, B.L., Timmermann, A., Bhattacharya, T., Rosenbloom, N., Brady, E., 2018. Glacial changes in tropical climate amplified by the Indian Ocean. Sci Adv 4, eaat9658.

Emile-Geay, J., McKay, N.P., Kaufman, D.S., von Gunten, L., Wang, J., Anchukaitis, K.J., Abram, N.J., Addison, J.A., Curran, M.A.J., Evans, M.N., Henley, B.J., Hao, Z., Martrat, B., McGregor, H.V., Neukom, R., Pederson, G.T., Stenni, B., Thirumalai, K., Werner, J.P., Xu, C., Divine, D.V., Dixon, B.C., Gergis, J., Mundo, I.A., Nakatsuka, T., Phipps, S.J., Routson, C.C., Steig, E.J., Tierney, J.E., Tyler, J.J., Allen, K.J., Bertler, N.A.N., Björklund, J., Chase, B.M., Chen, M.-T., Cook, E., de Jong, R., DeLong, K.L., Dixon, D.A., Ekaykin, A.A., Ersek, V., Filipsson, H.L., Francus, P., Freund, M.B., Frezzotti, M., Gaire, N.P., Gajewski, K., Ge, Q., Goosse, H., Gornostaeva, A., Grosjean, M., Horiuchi, K., Hormes, A., Husum, K., Isaksson, E., Kandasamy, S., Kawamura, K., Kilbourne, K.H., Koç, N., Leduc, G., Linderholm, H.W., Lorrey, A.M., Mikhalenko, V., Mortyn, P.G., Motoyama, H., Moy, A.D., Mulvaney, R., Munz, P.M., Nash, D.J., Oerter, H., Opel, T., Orsi, A.J., Ovchinnikov, D.V., Porter, T.J., Roop, H.A., Saenger, C., Sano, M., Sauchyn, D., Saunders, K.M., Seidenkrantz, M.-S., Severi, M., Shao, X., Sicre, M.-A., Sigl, M., Sinclair, K., St George, S., St Jacques, J.-M., Thamban, M., Kuwar Thapa, U., Thomas, E.R., Turney, C., Uemura, R., Viau, A.E., Vladimirova, D.O., Wahl, E.R., White, J.W.C., Yu, Z., Zinke, J., Consortium, P.A.k., 2017. A global multiproxy database for temperature reconstructions of the Common Era. Sci Data 4, 170088.

Fudeyasu, H., Ichiyanagi, K., Yoshimura, K., Mori, S., Hamada, J.-I., Sakurai, N., Yamanaka, D., Matsumoto, J., Syamsudin, F., 2011. Effects of large-scale moisture transport and mesoscale processes on precipitation isotope ratios observed at Sumatera, Indonesia. J. Meteorol. Soc. Jpn. Ser. II 89A, 49–59.

Galewsky, Joseph, Steen-Larsen, Hans Christian, Field, Robert, Worden, John, Risi, Camille, Schneider, Matthias, 2016. Stable isotopes in atmospheric water vapor and applications to the hydrologic cycle. Rev. Geophys. 54 (4), 809–865. https://doi.org/10.1002/2015RG000512.

Griffiths, M.L., Drysdale, R.N., Gagan, M.K., Zhao, J.x., Ayliffe, L.K., Hellstrom, J.C., Hantoro, W.S., Frisia, S., Feng, Y.x., Cartwright, I., Pierre, E.S., Fischer, M.J., Suwargadi, B.W., 2009. Increasing Australian–Indonesian monsoon rainfall linked to early Holocene sea-level rise. Nat. Geosci. 2, 636–639.

He, C., Liu, Z., Otto-Bliesner, B.L., Brady, E.C., Zhu, C., Tomas, R., Clark, P.U., Zhu, J., Jahn, A., Gu, S., Zhang, J., Nusbaumer, J., Noone, D., Cheng, H., Wang, Y., Yan, M., Bao, Y., 2021. Hydroclimate footprint of pan-Asian monsoon water isotope during the last deglaciation. Sci Adv 7, eabe2611.

Hughes, A.L.C., Gyllencreutz, R., Lohne, Ø.S., Mangerud, J., Svendsen, J.I., 2016. The last Eurasian ice sheets – a chronological database and time-slice reconstruction, DATED-1. Boreas 45, 1–45.

Konecky, B., Russell, J., Bijaksana, S., 2016. Glacial aridity in central Indonesia coeval with intensified monsoon circulation. Earth Planet Sci. Lett. 437, 15–24.

Konecky, B.L., Noone, D.C., Cobb, K.M., 2019. The influence of competing hydroclimate processes on stable isotope ratios in tropical rainfall. Geophys. Res. Lett. 46, 1622–1633.

Krause, C.E., Gagan, M.K., Dunbar, G.B., Hantoro, W.S., Hellstrom, J.C., Cheng, H., Edwards, R.L., Suwargadi, B.W., Abram, N.J., Rifai, H., 2019. Spatio-temporal evolution of Australasian monsoon hydroclimate over the last 40,000 years. Earth Planet Sci. Lett. 513, 103–112.

Kurita, N., Ichiyanagi, K., Matsumoto, J., Yamanaka, M.D., Ohata, T., 2009. The relationship between the isotopic content of precipitation and the precipitation amount in tropical regions. J. Geochem. Explor. 102, 113–122.

Lee, S.-Y., Chiang, J.C.H., Chang, P., 2015. Tropical Pacific response to continental ice sheet topography. Clim. Dynam. 44, 2429–2446.

Li, T., Wang, B., Chang, C.P., Zhang, Y., 2003. A theory for the Indian ocean dipole–zonal mode. J. Atmos. Sci. 60, 2119–2135.

Liu, J., Milne, G.A., Kopp, R.E., Clark, P.U., Shennan, I., 2016. Sea-level constraints on the amplitude and source distribution of Meltwater Pulse 1A. Nat. Geosci. 9, 130–134.

Liu, Z., Otto-Bliesner, B.L., He, F., Brady, E.C., Tomas, R., Clark, P.U., Carlson, A.E., Lynch-Stieglitz, J., Curry, W., Brook, E., Erickson, D., Jacob, R., Kutzbach, J., Cheng, J., 2009. Transient simulation of last deglaciation with a New mechanism for Bolling-Allerod warming. Science 325, 310–314.

Lüthi, D., Le Floch, M., Bereiter, B., Blunier, T., Barnola, J.-M., Siegenthaler, U., Raynaud, D., Jouzel, J., Fischer, H., Kawamura, K., Stocker, T.F., 2008. High-resolution carbon dioxide concentration record 650,000–800,000 years before present. Nature 453, 379–382.

McGee, D., Donohoe, A., Marshall, J., Ferreira, D., 2014. Changes in ITCZ location and cross-equatorial heat transport at the last glacial Maximum, heinrich Stadial 1, and the mid-holocene. Earth Planet Sci. Lett. 390, 69–79.

Meckler, A.N., Clarkson, M.O., Cobb, K.M., Sodemann, H., Adkins, J.F., 2012. Interglacial hydroclimate in the tropical west Pacific through the late pleistocene. Science 336, 1301.

Moerman, J.W., Cobb, K.M., Adkins, J.F., Sodemann, H., Clark, B., Tuen, A.A., 2013. Diurnal to interannual rainfall δ18O variations in northern Borneo driven by regional hydrology. Earth Planet Sci. Lett. 369–370, 108–119.

Mohtadi, M., Prange, M., Schefuss, E., Jennerjahn, T.C., 2017. Late holocene slowdown of the Indian Ocean Walker circulation. Nat. Commun. 8.

Niedermeyer, E.M., Sessions, A.L., Feakins, S.J., Mohtadi, M., 2014. Hydroclimate of the western Indo-pacific warm pool during the past 24,000 years. Proc. Natl. Acad. Sci. Unit. States Am. 111, 9402.

Nusbaumer, Jesse, Wong, Tony, Bardeen, Charles, Noone, David, 2017. Evaluating hydrological processes in the community atmosphere model version 5 (CAM5) using stable isotope ratios of water. J. Adv. Model. Earth Syst. 9 (2), 949–977. https://doi.org/10.1002/2016MS000839.

Otto-Bliesner, Bette, Russell, James, Clark, Peter, Liu, Zhengyu, Overpeck, Jonathan, Konecky, Bronwen, deMenocal, Peter, Nicholson, Sharon, He, Feng, Lu, Zhengyao, 2014. Coherent changes of southeastern equatorial and northern African rainfall during the last deglaciation. Science 346 (6214), 1223–1227. https://doi.org/10.1126/science.1259531.

Partin, J.W., Cobb, K.M., Adkins, J.F., Clark, B., Fernandez, D.P., 2007. Millennial-scale trends in west Pacific warm pool hydrology since the Last Glacial Maximum. Nature 449, 452–U453.

Peltier, W.R., Argus, D.F., Drummond, R., 2015. Space geodesy constrains ice age terminal deglaciation: the global ICE-6G_C (VM5a) model. J. Geophys. Res.: Solid Earth 120, 450–487.

Petit, J.R., Jouzel, J., Raynaud, D., Barkov, N.I., Barnola, J.M., Basile, I., Bender, M., Chappellaz, J., Davis, M., Delaygue, G., Delmotte, M., Kotlyakov, V.M.,

Legrand, M., Lipenkov, V.Y., Lorius, C., PÉpin, L., Ritz, C., Saltzman, E., Stievenard, M., 1999. Climate and atmospheric history of the past 420,000 years from the Vostok ice core, Antarctica. Nature 399, 429–436.

Pico, T, McGee, D, Russell, J, Mitrovica, J, 2020. Recent constraints on MIS 3 sea level support role of continental shelf exposure as a control on Indo-Pacific hydroclimate. Paleoceanogr. Paleoclimatol. 35 (8), 1–10. https://doi.org/10.1029/2020PA003998.

Reeves, J.M., Barrows, T.T., Cohen, T.J., Kiem, A.S., Bostock, H.C., Fitzsimmons, K.E., Jansen, J.D., Kemp, J., Krause, C., Petherick, L., Phipps, S.J., 2013. Climate variability over the last 35,000 years recorded in marine and terrestrial archives in the Australian region: an OZ-INTIMATE compilation. Quat. Sci. Rev. 74, 21–34.

Rozanski, K., Araguás-Araguás, L., Gonfiantini, R., 1993. Isotopic patterns in modern global precipitation. Clim. Change Continental Isot. Record. 1–36.

Ruan, Y., Mohtadi, M., van der Kaars, S., Dupont, L.M., Hebbeln, D., Schefuß, E., 2019. Differential hydro-climatic evolution of East Javanese ecosystems over the past 22,000 years. Quat. Sci. Rev. 218, 49–60.

Russell, J.M., Vogel, H., Konecky, B.L., Bijaksana, S., Huang, Y.S., Melles, M., Wattrus, N., Costa, K., King, J.W., 2014. Glacial forcing of central Indonesian hydroclimate since 60,000 y BP. Proc. Natl. Acad. Sci. U. S. A 111, 5100–5105.

Sathiamurthy, E., Voris, H., 2006. Maps of Holocene Sea Level Transgression and Submerged Lakes on the Sunda Shelf.

Schilt, A., Baumgartner, M., Blunier, T., Schwander, J., Spahni, R., Fischer, H., Stocker, T.F., 2010. Glacial–interglacial and millennial-scale variations in the atmospheric nitrous oxide concentration during the last 800,000 years. Quat. Sci. Rev. 29, 182–192.

Thirumalai, Kaustubh, DiNezio, Pedro, Tierney, Jessica, Puy, Martin, Mohtadi, Mahyar, 2019. An El Niño Mode in the Glacial Indian Ocean? Paleoceanogr. Paleoclimatol. 34 (8), 1316–1327. https://doi.org/10.1029/2019PA003669.

Tian, Z., Li, T., Jiang, D., 2018. Strengthening and westward shift of the tropical pacific Walker circulation during the mid-holocene: PMIP simulation results. J. Clim. 31, 2283–2298.

Wicaksono, S.A., Russell, J.M., Holbourn, A., Kuhnt, W., 2017. Hydrological and vegetation shifts in the Wallacean region of central Indonesia since the last glacial Maximum. Quat. Sci. Rev. 157, 152–163.

Windler, G., Tierney, J.E., DiNezio, P.N., Gibson, K., Thunell, R., 2019. Shelf exposure influence on Indo-Pacific Warm Pool climate for the last 450,000 years. Earth Planet Sci. Lett. 516, 66–76.

Windler, G., Tierney, J.E., Zhu, J., Poulsen, C.J., 2020. Unraveling glacial hydroclimate in the Indo-pacific warm pool: perspectives from water isotopes. Paleoceanogr Paleocl 35, e2020PA003985.

Winnick, M.J., Chamberlain, C.P., Caves, J.K., Welker, J.M., 2014. Quantifying the isotopic 'continental effect'. Earth Planet Sci. Lett. 406, 123–133.

Wong, Tony, Nusbaumer, Jesse, Noone, David, 2017. Evaluation of modeled land-atmosphere exchanges with a comprehensive water isotope fractionation scheme in version 4 of the community land model. J. Adv. Model. Earth Syst. 9 (2), 978–1001. https://doi.org/10.1002/2016MS000842.

Wurtzel, J.B., Abram, N.J., Lewis, S.C., Bajo, P., Hellstrom, J.C., Troitzsch, U., Heslop, D., 2018. Tropical Indo-Pacific hydroclimate response to North Atlantic forcing during the last deglaciation as recorded by a speleothem from Sumatra, Indonesia. Earth Planet Sci. Lett. 492, 264–278.

Zhu, J, Liu, Z, Brady, E, Otto-Bliesner, B, Zhang, J, Noone, D, Tomas, R, Nusbaumer, J, Wong, T, Jahn, A, Tabor, C, 2017. Reduced ENSO variability at the LGM revealed by an isotope-enabled Earth system model. Geophys. Res. Lett. 44 (13), 6984–6992. https://doi.org/10.1002/2017gl073406.